

The following resources related to this article are available online at www.sciencemag.org (this information is current as of November 4, 2009):

Updated information and services, including high-resolution figures, can be found in the online version of this article at:

<http://www.sciencemag.org/cgi/content/full/286/5442/1127>

This article **cites 11 articles**, 2 of which can be accessed for free:

<http://www.sciencemag.org/cgi/content/full/286/5442/1127#otherarticles>

This article has been **cited by** 867 article(s) on the ISI Web of Science.

This article appears in the following **subject collections**:

Materials Science

http://www.sciencemag.org/cgi/collection/mat_sci

Information about obtaining **reprints** of this article or about obtaining **permission to reproduce this article** in whole or in part can be found at:

<http://www.sciencemag.org/about/permissions.dtl>

- Oecologia* **110**, 449 (1997)]. The analysis and ecological interpretation of this issue are complex, but low levels of cover in the unmanipulated reference plots at some of our sites (sometimes 50% at the annual-dominated Portuguese field site) provide evidence against the automatic exclusion of plots with low cover.
25. J. H. Lawton, *Oikos* **71**, 367 (1994); S. Naeem, J. H. Lawton, L. J. Lindsey, S. P. Lawler, R. M. Woodfin, *Endeavour* **19**, 58 (1995); F. Schläpfer, B. Schmid, I. Seidl, *Oikos* **84**, 346 (1999).
 26. Data from the third year of the experiment have been processed for all sites except Portugal. Although there still appears to be no response in Greece, much of the other variation shown in Fig. 2 has disappeared, and the overall pattern appears to match the general log-linear relation more closely than in year two.
 27. D. A. Wardle, O. Zackrisson, G. Hörnberg, C. Gallet, *Science* **277**, 1296 (1997); D. Tilman *et al.*, *Science* **278**, 1866 (1997).
 28. Composition effects are a combination of the effects of particular species and of interactions between species in polycultures. An assemblage-by-location interaction indicated that where the same species or mixture of species occurred at more than one site, they generally achieved significantly different biomasses at different locations [$F_{29,235} = 3.77$, $P < 0.001$ (Table 3)].
 29. Each species or functional group was added individually to the multiple regression models in Table 3. Fitting each species or group separately meant that the effect attributed to each was maximized. Our ability to test the effects of the grass functional group was limited, because most of the assemblages included grasses.
 30. E. Garnier, M.-L. Navas, M. P. Austin, J. M. Lilley, R. M. Gifford, *Acta Oecol.* **18**, 657 (1997).
 31. We performed simple regressions of the estimated per-plant biomass of 14 species across a gradient of increasing species richness (on a \log_2 scale) after adjusting for differences between locations and blocks by taking residuals from analyses with these terms [seven of the species showed significantly different responses at different sites (Table 4)]. We expected slopes of zero where intraspecific competition was equal to competition with other species and expected positive and negative slopes where it was more and less intense, respectively. Under the sampling hypothesis, we expected approximately equal distributions of positive and negative slopes. In contrast, 12 of the 14 species had slopes that were positive; 8 significantly so. Two species had slopes that were negative, but neither was significantly different from zero.
 32. J. L. Harper, *Population Biology of Plants* (Academic Press, London, 1977).
 33. We identified the species with the highest biomass in each plant assemblage and, where data were available (271 of the 308 polycultures), compared their average monoculture biomass with the biomass of the total assemblage using the overyielding index D_{max} [M. Loreau, *Oikos* **82**, 600 (1998)], where $D_{max} = (\text{total biomass of a plant assemblage} - \text{average monoculture biomass of the dominant species in that assemblage}) / \text{average monoculture biomass of the dominant species in that assemblage}$. We analyzed D_{max} after transformation using natural logarithms (after adding 1 to make all values positive) to meet the assumptions of parametric analyses.
 34. The BIODEPTH project is funded by the European Commission within the Framework IV Environment and Climate program (ENV-CT95-0008). Many colleagues too numerous to list have assisted with the project; in particular, we thank P. Heads and E. Bazeley-White. We thank J. Nelder for advice on statistical analyses.

20 May 1999; accepted 14 September 1999

REPORTS

Hydrogen Storage in Single-Walled Carbon Nanotubes at Room Temperature

C. Liu,¹ Y. Y. Fan,¹ M. Liu,¹ H. T. Cong,² H. M. Cheng,^{1*}
M. S. Dresselhaus,^{3*}

Masses of single-walled carbon nanotubes (SWNTs) with a large mean diameter of about 1.85 nanometers, synthesized by a semicontinuous hydrogen arc discharge method, were employed for hydrogen adsorption experiments in their as-prepared and pretreated states. A hydrogen storage capacity of 4.2 weight percent, or a hydrogen to carbon atom ratio of 0.52, was achieved reproducibly at room temperature under a modestly high pressure (about 10 megapascal) for a SWNT sample of about 500 milligram weight that was soaked in hydrochloric acid and then heat-treated in vacuum. Moreover, 78.3 percent of the adsorbed hydrogen (3.3 weight percent) could be released under ambient pressure at room temperature, while the release of the residual stored hydrogen (0.9 weight percent) required some heating of the sample. Because the SWNTs can be easily produced and show reproducible and modestly high hydrogen uptake at room temperature, they show promise as an effective hydrogen storage material.

Hydrogen (H_2) has attracted a great deal of attention as an energy source. Once it is generated, its use as a fuel creates neither air pollution nor greenhouse gas emissions. However, no practical means for H_2 storage and transportation have yet been developed. Of the problems to be solved for the utilization of hydrogen energy, how to store H_2 easily and cheaply has been given high priority on the research agenda.

Recently, carbon nanotubes and carbon nanofibers were reported to be very promising candidates for H_2 uptake. Dillon *et al.* (1) first

measured the H_2 adsorption capacity of an as-prepared soot containing only about 0.1 to 0.2 weight % SWNTs at 133 K, from which they extrapolated an H_2 adsorptivity for pure SWNTs of 5 to 10 weight % (the weight of H_2 adsorbed divided by the weight of SWNTs plus the H_2 adsorbed by the SWNTs), and predicted that SWNTs with a diameter of between 1.63 and 2 nm would come close to the target H_2 uptake density of 6.5 weight %. Ye *et al.* (2) reported that a ratio of H to C atoms of about 1.0 was obtained for crystalline ropes of SWNTs at a cryogenic temperature of 80 K and

pressures >12 MPa. Instead of SWNTs, Chambers *et al.* (3) claimed that tubular, platelet, and herringbone forms of carbon nanofibers were capable of adsorbing in excess of 11, 45, and 67 weight % of H_2 , respectively, at room temperature and at a pressure of 12 MPa. More recently, Chen *et al.* (4) reported that a high H_2 uptake of 20 and 14 weight % can be achieved for Li-doped and K-doped multi-walled carbon nanotubes (MWNTs) in milligram quantities, respectively, under ambient pressure. The K-doped MWNTs can adsorb H_2 at room temperature, but they are chemically unstable, whereas the Li-doped MWNTs are chemically stable, but require elevated temperatures (473 to 673 K) for maximum adsorption and desorption of H_2 .

We measured the H_2 storage capacity of SWNTs synthesized by a hydrogen arc-discharge method, with a relatively large sample quantity (about 500 mg) at ambient temperature under a modestly high pressure. A H_2 uptake of 4.2 weight %, which corresponds to a H/C atom ratio of 0.52, was obtained by these SWNTs with an estimated purity of 50 weight %. Also, $\sim 80\%$ of the adsorbed H_2 can be released at room temperature. These results indicate that SWNTs are highly promising for H_2 adsorption even at room temperature.

¹Institute of Metal Research, Chinese Academy of Sciences, 72 Wenhua Road, Shenyang 110015, China.

²State Key Lab for Rapidly Solidified Non-equilibrium Alloys, Institute of Metal Research, Chinese Academy of Sciences, 72 Wenhua Road, Shenyang 110015, China. ³Department of Physics and Department of Electrical Engineering and Computer Science, Massachusetts Institute of Technology, Cambridge, MA 02139, USA.

*To whom correspondence should be addressed. E-mail: cheng@imr.ac.cn (H.M.C.) and millie@mgm.mit.edu (M.S.D.)

REPORTS

A semi-continuous hydrogen arc discharge technique was used for the synthesis of the SWNTs (5). In comparison to the traditional electric arc method (6), this method is characterized by (i) a large rotatable cylindrical anode (400 mm in diameter and 35 mm in height) composed of evenly dispersed graphite powder (94.5 atomic %), with Ni, Co, and Fe powders (3, 0.75, and 0.75 atomic %, respectively) as catalysts and FeS (1 atomic %) as a growth promoter. Furthermore, the electrodes are not vertically opposite each other, but rather make an oblique angle. (ii) H₂ rather than He gas was selected as a buffer gas. (iii) The addition of a sulfur-containing growth promoter was found to be critical. The rotatable large anode makes our synthesis procedure a semi-continuous one, and a yield of about 2 g of SWNTs per hour can be achieved reproducibly. There are mainly two kinds of products obtained: thin films that peeled off from the upper chamber wall and a web-like substance that hangs between the cathode and the upper chamber wall. Both kinds of products are lightweight and sticky. We show a high-resolution scanning electron microscope (HRSEM) image of the as-prepared thin-film substance (Fig. 1), in which SWNT bundles (~20 nm in diameter) that are entangled with one another can be observed. The results from thermogravimetric measurements showed that the content of the catalyst residue in our products was

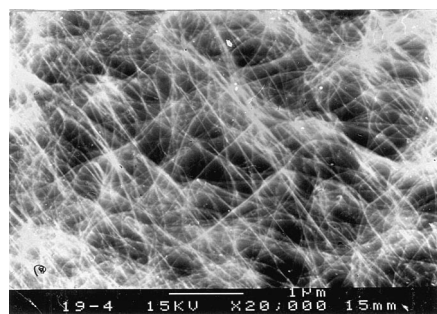


Fig. 1. HRSEM image of the as-prepared SWNTs.

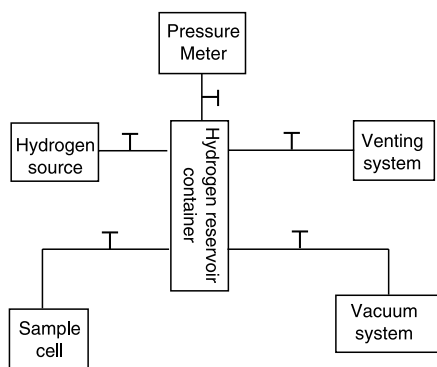


Fig. 2. The schematic diagram of the apparatus used for H₂ adsorption experiments.

~40 weight %, so the purity of our SWNTs may be in the range of 50 to 60 weight %. Results from Raman scattering measurements and HRSEM and high-resolution transmission electron microscope (HRTEM) observations were also performed to confirm the high quality of the products (5).

We carried out H₂ adsorption experiments with the as-prepared SWNTs, as well as with samples after some pretreatment. Three samples of SWNTs (each of ~500 mg in weight) were collected from a batch of as-prepared SWNTs, but were pretreated in three different ways, and then were denoted as sample 1, sample 2, and sample 3. Their pretreatment processing methods and the H₂ adsorption amounts are listed in Table 1. A schematic diagram of the apparatus used for the H₂ adsorption experiments is illustrated (Fig. 2). The apparatus consists of a copper sample cell, a stainless steel H₂ reservoir container, a H₂ source (99.999% in purity), a vacuum system, a high-pressure gauge, and high-pressure bellows valves through which the above components are all connected. The volume of the system was measured to be 45.10 ml. Blank experiments were done several times before and after the H₂ storage measurements to verify that the apparatus was leak-free.

In the H₂ adsorption experiments, each of the SWNT samples was placed in the sample cell and heated to 423 K. The system was then fully vacuum-degassed for several hours

(the vacuum in the sample cell was measured to be about 1.3 Pa torr in the control experiment). When the sample cell was cooled to room temperature (about 298 K), H₂ was admitted into the apparatus to a certain pressure (about 10 to 12 MPa) and the H₂ adsorption began. The changes in pressure were monitored versus time. The results for the H₂ adsorption in weight % are shown (Fig. 3) for the three samples that were measured. The adsorption rate decreases after the first 60 min, and at that time, ~70% of the whole adsorption capacity is achieved.

The H₂ storage capacities for the three samples, from highest capacity to lowest, are sample 3 > sample 2 > sample 1. Sample 2 was soaked in HCl acid (37%) for 48 hours to partly eliminate the residual catalysts and was then rinsed with de-ionized water; it showed a somewhat higher H₂ adsorption capacity than sample 1 (the as-prepared product). This indicates that catalyst particles are probably inert with regard to H₂ adsorption. Sample 3, in comparison to sample 2, was heat-treated in vacuum at 773 K for 2 hours after receiving the same pretreatment as sample 2. A large increase in adsorption capacity for sample 3 relative to samples 1 and 2 was observed (Fig. 3). The heat treatment in vacuum could evaporate organic compounds (such as naphthalene and anthracene) and organic functional groups that had formed on the surface of SWNTs during the synthesis pro-

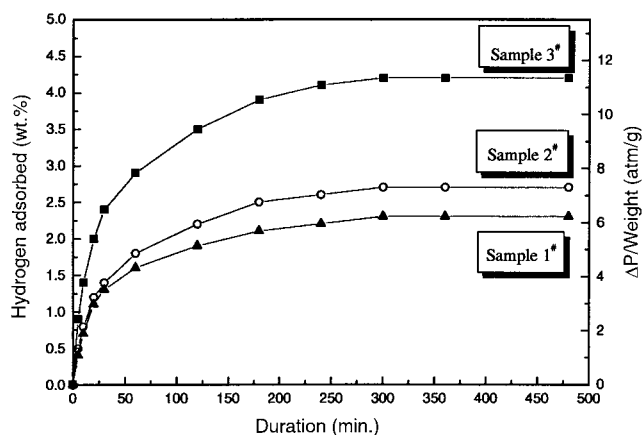


Fig. 3. The amount of H₂ in weight % for SWNT samples, and the pressure change versus the adsorption time.

Table 1. Uptake of H₂ for three samples. Sample 1 was used as-synthesized. Sample 2 was soaked in 37% HCl acid for 48 hours, rinsed with deionized water, and dried at 423 K. Sample 3 was pretreated in the same way as sample 2, then vacuum heat-treated for 2 hours at 773 K. All samples were placed in the sample cell, heated at 423 K, degassed in vacuum for several hours, and then exposed to 100 to 120 atm of H₂ at 298 K until equilibrium was achieved (typically 6 hours). The storage capacity we report is based on the pressure changes described above. After the samples were returned to ambient pressure, some of the hydrogen was found to not desorb; this residual hydrogen storage (at room temperature) is expressed as a percentage of the total storage capacity. The values reported have an error of <0.38 weight %.

Sample	Storage capacity (weight %)	Initial mass (mg)	Final mass (mg)	Residual H ₂ storage (%)
1	2.4	480.1	482.6	21.2
2	2.8	501.3	504.9	24.9
3	4.2	492.7	497.4	21.7

cedure and acid washing. In fact, almost no organic substances could be detected by gas chromatography–mass spectrometry after the vacuum heat treatment. These results indicate that the surface pretreatment of the sample is of great importance for improving the H₂ storage capacity of SWNTs, and systematic investigations of the pretreatment need to be carried out.

After adsorption equilibrium was achieved, the H₂ in the system was vented. The samples were then brought out and weighed, the results of which are shown in Table 1. There was a weight increase (0.5 to 1 weight %) for all three samples even after the stored H₂ was desorbed at room temperature. This implies that a certain amount of H₂ storage (21 to 25% of the total adsorbed H₂) could not be desorbed at ambient pressure and temperature. We tried heating these samples at 473 K and found that the weight increase disappeared, showing that essentially all the H₂ can be desorbed at elevated temperatures. This part of the residual H₂ may be related to chemical adsorption, which requires a higher energy for desorption. A few H₂ adsorption/desorption cycles were also carried out using the same experimental apparatus and parameters. The results show that after four cycles of adsorption/desorption, the H₂ uptake capacity of the SWNTs remained almost unchanged. The H₂ pressure has a great influence on its storage in the SWNTs. It was found that only a small amount of H₂ (less than 1 weight %) can be stored at pressures lower than 5 MPa, which is consistent with the results obtained at a cryogenic temperature of 80 K by Ye *et al.* (2).

The SWNT purity for sample 3 was estimated to be about 50 to 60 weight % from the results of thermogravimetric measurements and microscopic observations. It can then be expected that the H₂ adsorption capacity of pure SWNTs will likely be larger than 4.2 weight % even at room temperature under modestly high pressure. We argue that this relatively high H₂ adsorption capacity of our SWNTs may be related to their larger mean diameter. The results from our HRTEM observations show that our SWNTs have a mean diameter of 1.85 ± 0.05 nm, while typical SWNT diameters are in the range of about 1.2 to 1.4 nm (6, 7). From the Raman scattering spectrum of the sample, we found main peaks at 121 and 138 cm⁻¹ in the low-frequency band, which was down-shifted from the corresponding Raman band for the SWNTs synthesized by the laser ablation method (7). These low-frequency peaks are considered to be related to the radial breathing mode (RBM) vibration of SWNTs, and the frequency of this radial mode is inversely proportional to the diameter of the SWNTs (8). The diameter of our SWNTs was determined by the Raman effect to be 1.85 and 1.62 nm, respectively, for the RBM peaks of 121 and

138 cm⁻¹, calculated from the equation of $\omega = 223.75/d$ given by Bandow *et al.* (8), where ω is the frequency of the RBM of SWNTs in units of centimeters⁻¹ and d is the diameter of the SWNTs in nanometers. These results are therefore consistent with the HRTEM-observed diameter for our SWNTs. According to theoretical estimates, SWNTs with a larger mean diameter will allow greater H₂ storage (1, 9). The larger mean diameter of our SWNTs can be attributed to the addition of a sulfur-containing growth promoter (10, 11), which is a characteristic of our synthesis technique.

Although a H₂ adsorption capacity of 4.2 weight % was achieved at room temperature under modestly high pressure on the SWNTs synthesized by a semi-continuous hydrogen arc discharge method, further investigations are needed for this potentially high-capacity H₂ storage material.

References and Notes

1. A. C. Dillon *et al.*, *Nature* **386**, 377 (1997).
2. Y. Ye *et al.*, *Appl. Phys. Lett.* **74**, 2307 (1999).
3. A. Chambers, C. Park, R. T. K. Baker, N. M. Rodriguez, *J. Phys. Chem. B* **122**, 4253 (1998).
4. P. Chen, X. Wu, J. Lin, K. L. Tan, *Science* **285**, 91 (1999).
5. C. Liu *et al.*, *Carbon*, **37**, 1865 (1999).
6. C. Journet *et al.*, *Nature* **388**, 756 (1997).
7. A. M. Rao *et al.*, *Science* **275**, 187 (1997).
8. S. Bandow *et al.*, *Phys. Rev. Lett.* **80**, 3779 (1998).
9. S. D. M. Brown, G. Dresselhaus, M. S. Dresselhaus, *Mater. Res. Soc. Symp. Proc.* **497**, 157 (1998).
10. C. H. Kiang, W. A. Goddard III, R. Beyers, D. S. Bethune, *Carbon* **33**, 903 (1995).
11. H. M. Cheng *et al.*, *Chem. Phys. Lett.* **289**, 602 (1998).
12. We thank G. Dresselhaus, S. D. M. Brown, R. T. Yang, M. R. Black, and G. Su for their stimulating discussions. H.M.C. thanks National Natural Science Foundation of China for research grants 59872045 and 59672024, and the High-Tech Program of the Ministry of Science and Technology (MOST) of China. M.S.D. acknowledges support from NSF grant DMR 98-04734.

27 July 1999; accepted 4 October 1999

Polycationic Peptides from Diatom Biosilica That Direct Silica Nanosphere Formation

Nils Kröger,* Rainer Deutzmann, Manfred Sumper

Diatom cell walls are regarded as a paradigm for controlled production of nanostructured silica, but the mechanisms allowing biosilicification to proceed at ambient temperature at high rates have remained enigmatic. A set of polycationic peptides (called silaffins) isolated from diatom cell walls were shown to generate networks of silica nanospheres within seconds when added to a solution of silicic acid. Silaffins contain covalently modified lysine-lysine elements. The first lysine bears a polyamine consisting of 6 to 11 repeats of the *N*-methyl-propylamine unit. The second lysine was identified as ϵ -*N*,*N*-dimethyl-lysine. These modifications drastically influence the silica-precipitating activity of silaffins.

The chemical synthesis of silica-based materials like resins, molecular sieves, and catalysts requires extremes of temperature, pressure, and pH. In contrast, biosilicification proceeds at ambient temperatures and pressures, producing an amazing diversity of nanostructured frameworks (1–4). The silica cell wall of diatoms consists of two overlapping valves, and their structure is precisely controlled by the cell. During cell division a new valve is formed in minutes by controlled precipitation of silica within a specialized membrane vesicle called silica deposition vesicle (SDV) (5). Electron microscopic evidence indicates that the silica is initially deposited in the form of nanoscale spheres, suggesting the presence of components within the diatom cell that control silica sphere

formation (6, 7). However, the molecular structure of these components has remained elusive. It is well established that amorphous silica in diatom cell walls is intimately associated with organic substances that have been hypothesized to act as regulating molecules in biosilicification (8–10).

We examined the protein composition of cell walls from the diatom *Cylindrotheca fusiformis* (Fig. 1). Extraction of purified cell walls with EDTA led to the characterization of a Ca²⁺-binding protein family called frustulins (11). Even after harsh extraction procedures with boiling SDS solutions the resulting silica preparation still contains tightly bound organic material that is recovered only after solubilizing silica with anhydrous hydrogen fluoride (HF). This HF-extractable material consists of two main protein fractions: a high molecular mass protein family, termed HEPs, that is localized at a specific substructure of the cell wall (12), and a low molecular mass fraction with apparent

Lehrstuhl Biochemie I, Universität Regensburg, 93053 Regensburg, Germany.

*To whom correspondence should be addressed. E-mail: nils.kroeger@vkl.uni-regensburg.de